Simulating gas–liquid–water partitioning and fluid properties of petroleum under pressure: Implications for deep-sea blowouts

—

Supporting Information

*Jonas Gros;[1,2] Christopher M. Reddy;[3] Robert K. Nelson;[3] Scott A. Socolofsky;[4] and J. Samuel Arey[1,2]**

[1] Environmental Chemistry Modeling Laboratory (LMCE), GR C2 544, School of Architecture, Civil and Environmental Engineering, Ecole Polytechnique Fédérale de Lausanne (EPFL), Station 2, CH-1015 Lausanne, Switzerland

[2] Eawag, Swiss Federal Institute of Aquatic Science and Technology, Überlandstrasse 133, CH-8600 Dübendorf, Switzerland

[3] Department of Marine Chemistry & Geochemistry, Woods Hole Oceanographic Institution, Woods Hole, MA 02543, USA

[4] Zachry Department of Civil Engineering, Texas A&M University, College Station, TX 77843, USA

This document provides: Estimated contours of the air-water partition coefficient and vapor pressure overlaid on the GC×GC–FID chromatogram space (section S-1); description of the PR EOS (section S-2); procedure for gas-liquid-water equilibrium calculations (section S-3); comparison of the reported $<C_5$ compositions among different MRF samples (section S-4); procedure to combine gas phase analysis and simulated distillation data (section S-5); GC×GC–FID instrument method (section S-6); chemical structures of GC×GC–FID pseudocomponents (section S-7); definition of pseudocomponents for single carbon number intervals (section S-8); definition of $MC_{1,do}$ (section S-9); detailed definitions of MC_2 and MC_3 (section S-10); procedure to select literature Henry's law data (section S-11); validation of group contribution methods (section S-12); data used to test eqs 6 and 7 (section S-13); detailed explanation of differences between our thermodynamic model and the Zick model (section S-14); thermodynamic model validation (section S-15); model domain of validity (section S-16); and discussion of the model-predicted change in density due to evaporation and aqueous dissolution for $MC_{1,do}$ (section S-17).

(35 pages)

S-1 Estimated contours of air-water partition coefficient and vapor pressure overlaid on the GC×GC–FID chromatogram of sample MW-1

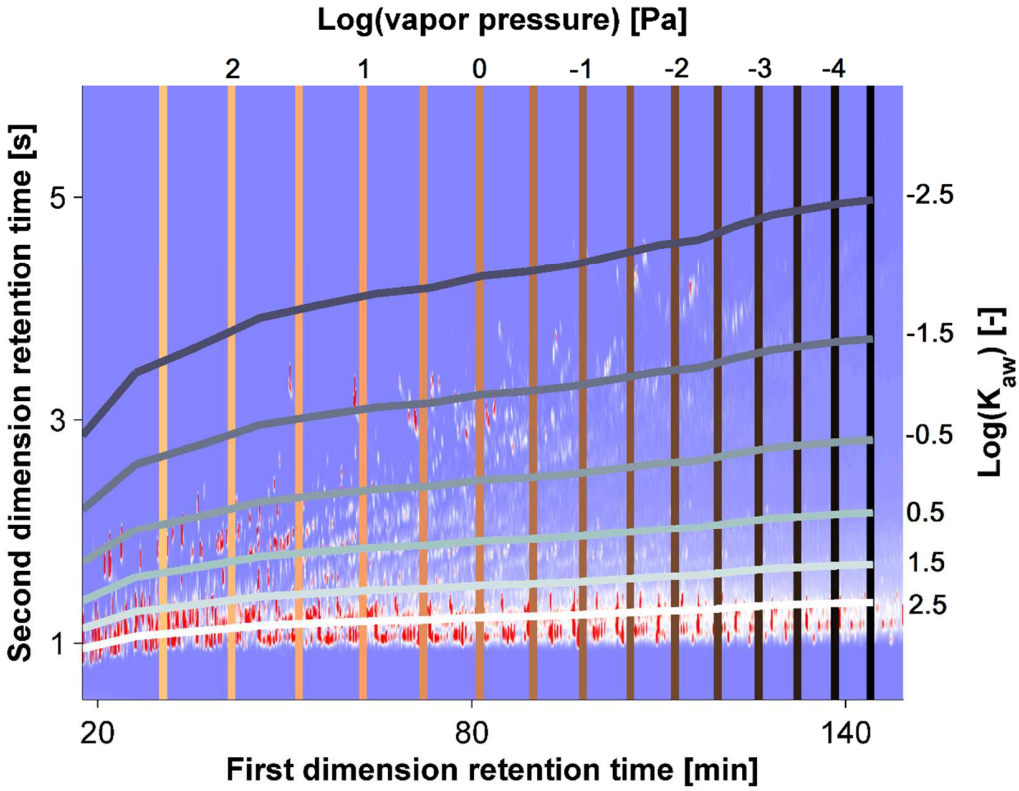

Figure S-1. GC×GC–FID chromatogram of MW-1 dead oil overlaid with estimated contours of the base 10 logarithm of decreasing vapor pressure (from left to right) and base 10 logarithm of increasing air-water partition coefficient, K_{aw} (from top to bottom). These lines were drawn by use of the Matlab[1] algorithms of Nabi et al.[2] K_{aw} is expressed here in units of (mol m^{-3}) (mol m^{-3})$^{-1}$, i.e. concentration in gas phase divided by concentration in aqueous phase. The relation between K_{aw} and the Henry's law constant K_H, here defined as in kg m^{-3} Pa^{-1}, is: $K_{H,i} = \frac{M_i}{R \cdot T} \cdot \left(K_{aw,i}\right)^{-1}$, where M_i is the molar weight of compound i in kg mol^{-1}, R is the molar gas constant (8.314510 J mol^{-1} K^{-1}), and T is the temperature in K.

S-2 Further description of the terms in the Peng-Robinson equation of state

Eq 1 can be rewritten as a 3rd degree polynomial of the compressibility factor, *Z*:

$$Z^3-(1-B)\cdot Z^2+(A-3\cdot B^2-2\cdot B)\cdot Z-(A\cdot B-B^2-B^3)=0 \quad \text{(eq. S-1)}$$

where:

$$Z=\frac{P\cdot \overline{V}}{R\cdot T} \quad \text{(eq. S-2)}$$

$$A=\frac{a\cdot P}{R^2\cdot T^2} \quad \text{(eq. S-3)}$$

$$B=\frac{b\cdot P}{R\cdot T} \quad \text{(eq. S-4)}$$

where *P* refers to the (total system) pressure, *T* is the temperature, *R* is the molar gas constant, $\overline{V}$ is the molar volume, and *a* and *b* are defined by eqs S-5 to S-11 below.

$$b_i(T)=b_i(T_{c,i})=0.07780\cdot\frac{R\cdot T_{c,i}}{P_{c,i}} \quad \text{(eq. S-5)}$$

where $P_{c,i}$ refers to the critical pressure of component *i*, and $T_{c,i}$ is the critical temperature of component *i*.

$$a_i(T)=a_i(T_{c,i})\cdot\alpha_i(T_{r,i},\omega_i)=0.45724\cdot\frac{R^2\cdot {T_{c,i}}^2}{P_{c,i}}\cdot\alpha(T_{r,i},\omega_i) \quad \text{(eq. S-6)}$$

where $T_{r,i}$ refers to the reduced temperature of component *i* $\left(T_{r,i}=\frac{T}{T_{c,i}}\right)$, and ω_i is the acentric factor of component *i*.

$$\alpha_i(T_{r,i},\omega_i)=\left(1+\kappa_i(\omega_i)\cdot\left(1-{T_{r,i}}^{0.5}\right)\right)^2 \quad \text{(eq. S-7)}$$

$$\kappa_i(\omega_i)=\begin{cases}0.37464+1.54226\cdot\omega_i-0.26992\cdot\omega_i^2 & (\omega_i\le 0.49)\\ 0.379642+1.48503\cdot\omega_i-0.164423\cdot\omega_i^2+0.016666\cdot\omega_i^3 & (\omega_i>0.49)\end{cases} \quad \text{(eq. S-8)}$$

$$a_{i,j}(T)=\left(1-\delta_{i,j}\right)\cdot a_i(T)^{0.5}\cdot a_j(T)^{0.5} \quad \text{(eq. S-9)}$$

where $\delta_{i,j}$ refers to the binary interaction parameter for components *i* and *j*.

$$a = \sum_i \sum_j \left(x_i \cdot x_j \cdot a_{i,j}(T) \right) \qquad \text{(eq. S-10)}$$

where x_i refers to mole fraction of component *i* in the mixture, and x_j refers to mole fraction of component *j* in the mixture.

$$b = \sum_i \left(x_i \cdot b_i \right) \qquad \text{(eq. S-11)}$$

Depending on the number of phases present, eq S-1 has one to three roots in terms of *Z*. In the two-phase region, the smallest positive root corresponds to the compressibility factor of the liquid, and the largest root corresponds to that of the gas phase.

Volume translation can be applied to the PR EOS:

$$\overline{V}_{VT} = \overline{V}_{PR\ EOS} - c \qquad \text{(eq. S-12)}$$

where the corrected molar volume, $\overline{V}_{VT}$, is obtained by adjusting the molar volume predicted by the equation of state, $\overline{V}_{PR\ EOS}$, with the volume translation parameter, *c*.

Fugacities of individual components in the two (gas and liquid) phases, f_i, are computed from:[3]

$$\ln\left(f_i\right) = \ln\left(x_i \cdot P\right) + \frac{b_i}{b} \cdot \left(Z - 1\right) - \ln\left(Z - B\right) - \frac{A}{2 \cdot \sqrt{2} \cdot B} \cdot \left(\frac{2 \cdot \sum_j \left(x_j \cdot a_{i,j} \right)}{a} - \frac{b_i}{b} \cdot \right) \cdot \ln\left(\frac{Z + 2.414 \cdot B}{Z - 0.414 \cdot B} \right) \qquad \text{(eq. S-13)}$$

S-3 Procedure for gas-liquid-water equilibrium calculation

The general procedure of our gas-liquid-water equilibrium calculation is described in Figure S-2. Each step is detailed further below.

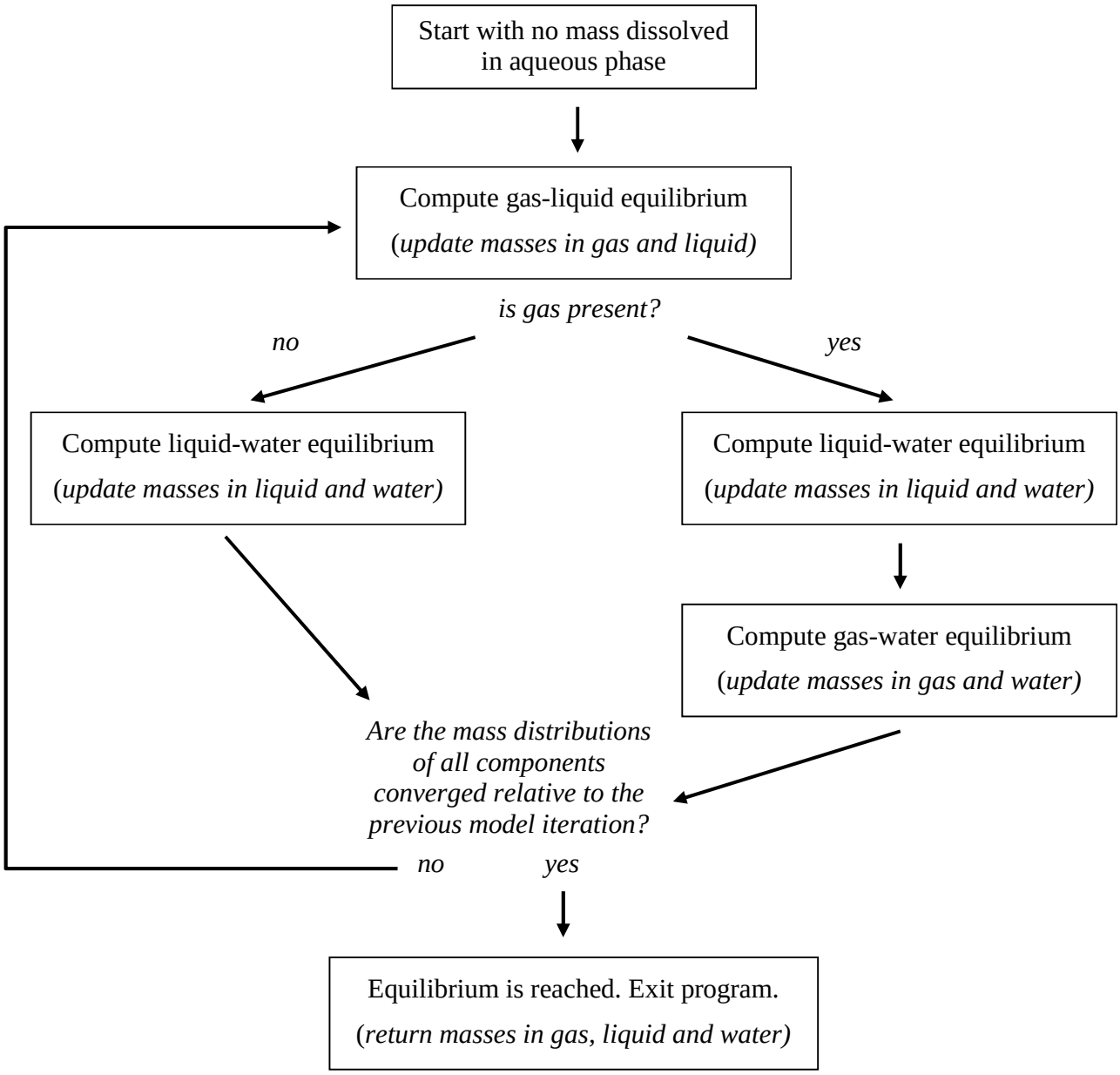

Figure S-2. Schematic representation of our gas-liquid-water equilibrium calculation procedure.

Convergence of gas-liquid equilibrium computations

The gas-liquid equilibrium calculation is performed using a combination of successive substitution, stability analysis, and second order minimization techniques.[4] We follow the overall procedure outlined on pages 266–267 of reference 4.

Successive substitution relies on so-called "K-factors", defined as:

$$K_i = \frac{y_i}{x_i} = \frac{\phi_{liq,i}}{\phi_{gas,i}} \qquad \text{(eq. S-14)}$$

where K_i is the K-factor of component i, y_i and x_i are mole fractions of component i in the gas and liquid phases, respectively, and $\phi_{gas,i}$ and $\phi_{liq,i}$ are fugacity coefficients of component i in the gas and liquid phases, respectively.

An initial guess for K-factors is obtained from the Wilson correlation (page 259 of reference 4). Successive substitution consists of using the current K-factor estimates to determine the new y_i and x_i values (procedure at pages 253–254 of reference 4, where we chose the tolerance value for convergence to be 10^{-6}). Fugacity coefficients are then computed from y_i and x_i, using the PR EOS, which allows the determination of an updated K-factor estimate ($K_i = \phi_{liq,i} / \phi_{gas,i}$). The procedure is repeated iteratively.

Initially, three steps of successive substitution are performed, after which the difference in Gibbs energy of the resulting vapor and liquid compared to the single-phase mixture is evaluated. Different procedures are followed depending on the outcome of this evaluation (cases a–c on page 266 of reference 4). In favorable cases, the equilibrium calculation can be converged rapidly with additional steps of successive substitution (convergence was evaluated using the error function defined by equation 15-31 at page 430 of reference 5 with a convergence criterion set to $1.49012 \cdot 10^{-8}$). In other cases, a tangent plane stability analysis is performed, which is a procedure to verify whether two phases are thermodynamically stable, or whether only one phase is present (pages 267–270 of reference 4); convergence for stability analysis is evaluated by verifying that the sum of the absolute values of the left-hand side of equation 46 on page 267 of reference 4 becomes smaller than 10^{-6}. When the rate of convergence becomes too low (which we defined by a number of iterations larger than $40 \cdot n_c$, where n_c is the number of components in the mixture), we switch to second order minimization techniques (pages 262–263 and 269 of reference 4).

Finally, after the three initial steps of successive substitution, any time that successive substitution reaches a stage where the current K-factor estimate indicates a single-phase mixture (i.e. that the fraction of the total moles in the gas phase obtained from the procedure at pages 253–254 of reference 4 is 0 or 1), a stability analysis is conducted to confirm this outcome or provide an improved estimate for the K-factors (page 267 of reference 4).

Any phase with $<10^{-5}$ times the total number of moles in the mixture is assumed negligible (i.e. in such cases the mixture is assumed single-phase).

Convergence of liquid-water and gas-water equilibrium computations

Initially, Henry's law constants are corrected for pressure, temperature, and salinity (eqs 3–5 in main text). Then, an iterative procedure is started. Fugacities in the petroleum gas or liquid phases can be computed from the PR EOS (eq S-13), and the aqueous saturation concentration of component *i*, $C_{s,i}$, is simply obtained as:

$$C_{s,i} = f_i \cdot K_{H,i} \qquad \text{(eq. S-15)}$$

where f_i is the fugacity of component *i* in the petroleum gas or liquid phase, and $K_{H,i}$ is the Henry's law constant of component *i* (corrected for pressure, temperature and salinity). The mass dissolved at each iteration is obtained as $\Delta m_{diss,i} = (C_{s,i} - C_{water,i}) \cdot V_{water} \cdot \lambda$. $C_{water,i}$ is the concentration of component *i* in the water from the previous iteration, V_{water} is the volume of water, and λ is a parameter that has a value of 1 at first iteration, and its value is divided by two when the iterative decrease in the change in composition is <1% for any of the total mass dissolved in water, methane, ethane, or propane (the minimal value of λ is set to 1/128). The amount of mass obtained for each component is transferred to the aqueous phase, and the masses in the petroleum gas or liquid phase are updated accordingly. This procedure is repeated for at least 10 iterations and at maximum $1/\lambda$ iterations.

Convergence criterion for the gas-liquid-water equilibrium calculation

Convergence of the gas-liquid-water equilibrium calculation is assumed to be reached when two criteria are both reached: the total mass dissolved in water changes by <0.5% between two consecutive iterations; and the individual masses dissolved in water for methane, ethane, and propane are changed by <0.05% between two consecutive iterations.

S-4 Comparison of the composition of light compounds in MW-1 versus pre-spill downhole single-phase Macondo reservoir fluid (MRF) samples

We investigated whether biased sampling could explain the reportedly lower value of the gas-to-oil ratio (GOR) of the MW-1 sample, relative to the pre-spill downhole samples. In this section, we will demonstrate that the available data does not support this hypothesis. The pre-spill downhole samples were taken at pressure and temperature conditions (81.7 MPa and 390 K) indicating a single-phase mixture. However for MW-1 sample, the local conditions indicated that the mixture had separated into two phases. At the MW-1 sampling conditions, light compounds will tend to partition into the gas phase in larger proportion than heavier compounds. As a result, a hypothetical sampling bias towards the petroleum liquid phase in the MW-1 sample would produce a lower relative concentration of the lowest molecular weight compounds compared to the higher molecular weight compounds, especially for C_1–C_5. However, the measured C_1–C_5 data do not appear to exhibit any systematic fractionation pattern in one sample compared to the other (Fig. S-3), which suggests that sampling bias towards the liquid phase is not a likely explanation of the overall compositional discrepancy. As a result, we consider the two different sources of compositional information (MW-1 and pre-spill downhole samples) as equally valid.

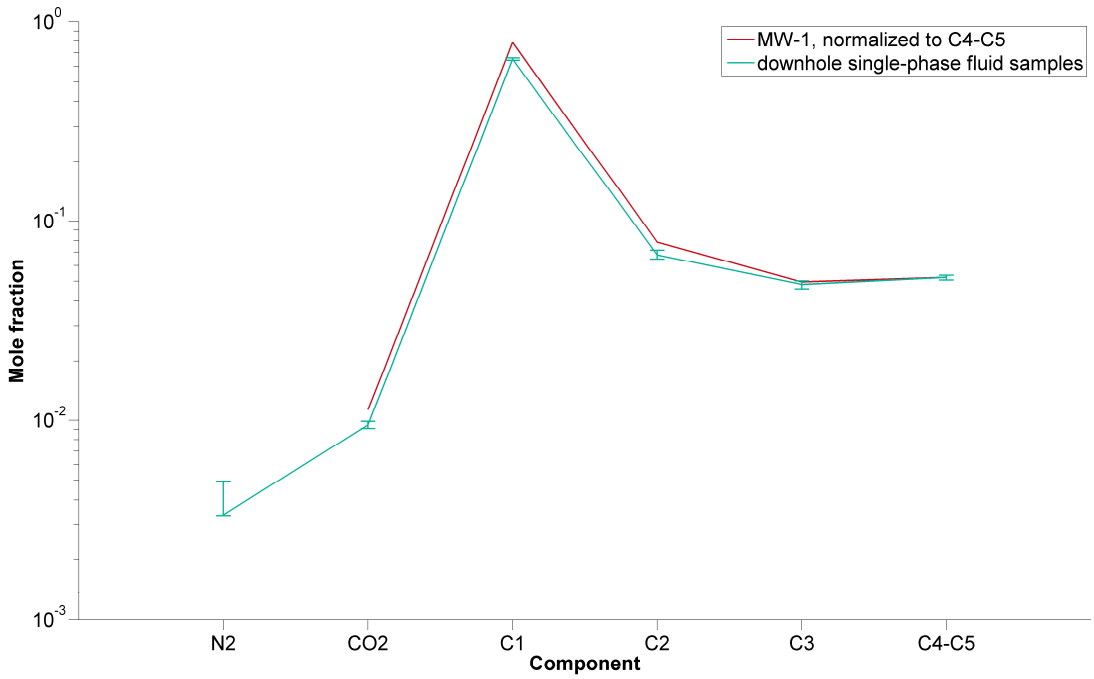

Figure S-3. Comparison of reported N_2, CO_2, and C_1–C_5 hydrocarbon content between different reservoir fluid samples. The "average" pre-spill downhole sample composition is defined by Zick as the average of the heaviest and lightest pre-spill downhole samples,[6] with error bars showing the range of values for the four sample compositions provided in his Table 2. The composition of the MW-1 sample is normalized so that the C_4–C_5 mole fraction matches the average of the lightest and heaviest pre-spill downhole single-phase fluid samples.

S-5 Combining light hydrocarbon and dead oil composition data

To obtain the mass fractions of carbon number intervals from C_1 to C_{108}, results from the compositional analysis of the gas phase and dead oil must be combined. To construct the model mixture MC_1, we used the listed mass fractions in Macondo reservoir fluid (MRF) from Table S2 in Reddy et al. for the C_1–C_5 hydrocarbon compounds and CO_2.[7] We used the simulated distillation data (mass fraction in dead oil for each single carbon number interval) in the C_6–C_{108} range. The mass fraction of C_6–C_{108} dead oil to mass fraction of MRF was assumed to have a ratio of 0.757:1.[7] The mass fractions of single carbon number intervals for the pre-spill downhole single-phase MRF samples were obtained as described in SI Section S-10.

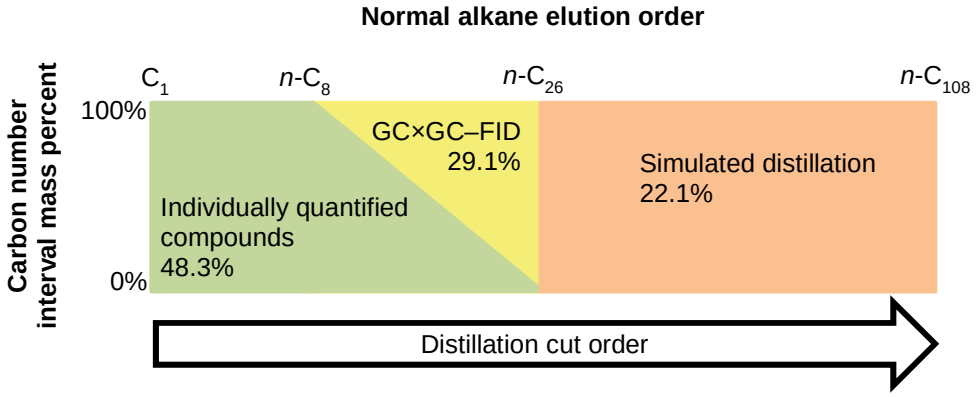

Figure S-4. Schematic summary of existing knowledge about the composition of MRF. Nearly 100% of the mass of C_1 to *n*-C_8 hydrocarbons is characterized by the measured mass fractions of individually quantified known compounds (green). With increasing carbon number beyond *n*-C_8, individually quantified compounds represent a decreasing fraction of the mixture, and GC×GC–FID data (yellow) are used to provide pseudocomponents for compounds not quantified individually. Finally, compounds larger than *n*-C_{26} are characterized based on simulated distillation data (salmon color). Mass percentages in MW-1 for each category are displayed on the figure.

S-6 Comprehensive two-dimensional gas chromatography (GC×GC) analysis method

An aliquot of the dead oil separated from the MW-1 sample[7] was analyzed by GC×GC coupled to a flame ionization detector (GC×GC–FID).

The sample was injected splitless on a GC×GC–FID (Agilent 7890) having an Rxi-ms first-dimension column (60 m length, 0.25 mm internal diameter (I.D.), 0.25 μm film thickness) and a BPX-50 second-dimension column (1.5 m length, 0.10 mm I.D., 0.10 μm film thickness). The carrier gas was H_2 at a constant flow rate of 1.00 mL min^{-1}. The inlet temperature was held at 310 ºC. The first oven was programmed as follows: hold at 45 ºC for 10 min, ramp from 45 to 330 ºC at 1.50 ºC min^{-1} (held 0.50 min). The second oven was programmed to remain 5 °C warmer than the first oven throughout the run. The modulation period was 7.50 s. The modulator was maintained 10 °C warmer than the second

oven, with a hot pulse time of 0.75 s and cool time of 3.00 s. The FID was at 330 °C, and the detector acquisition rate was 100 Hz, with a 1000 s acquisition delay.

For the quantification of the total (resolved plus unresolved) signal,[8] we have shown previously that it is appropriate to baseline-correct the chromatogram[8,9] with the deadband method of Reichenbach and co-workers.[10] We used GC Image (version 2.2b4)[11] with the following parameters: 10 deadband pixels per modulation; filter window size of 3 pixels, 3.5 for the expected value of baseline plus noise to the estimated standard deviation of the noise; and one baseline value per modulation.

S-7 Approximate chemical structures assigned to pseudocomponents derived from GC×GC–FID

The rules employed to assign approximate structures to pseudocomponents are the following:

- **Saturated hydrocarbons** are modeled as a normal alkane with varying chain length, from *n*-C_9 to *n*-C_{26}.
- **1-ring aromatic hydrocarbons** are modeled as a linear alkyl benzene with varying alkyl chain length, from ethylbenzene to nonadecylbenzene.
- **2-ring aromatic hydrocarbons** are modeled as a naphthalene structure with different degrees of methylation. The smallest 2-ring structure assigned is that of naphthalene, and each increase of one carbon atom corresponds to the addition of a methyl group. When no more methyl groups can be added, one of the methyl chain is converted to an ethyl group and subsequently to longer linear chain groups (propyl, butyl, …) for each carbon number increase.
- **3-ring aromatic hydrocarbons** are modeled as a phenanthrene structure with different degrees of methylation. The smallest 3-ring structure assigned is that of phenanthrene, and each increase of one carbon atom corresponds to the addition of a methyl group.
- **4-ring aromatic hydrocarbons** are modeled as a pyrene structure with different degrees of methylation. The smallest 4-ring structure assigned is that of pyrene, and each increase of one carbon atom corresponds to the addition of a methyl group.

The reader is referred to Fig. 1b (main text) for a few examples of the assigned approximate structures. A key indicating the assumed structure of each pseudocomponent obtained from the GC×GC–FID chromatogram is provided by Fig. S-5 and Table S-1.

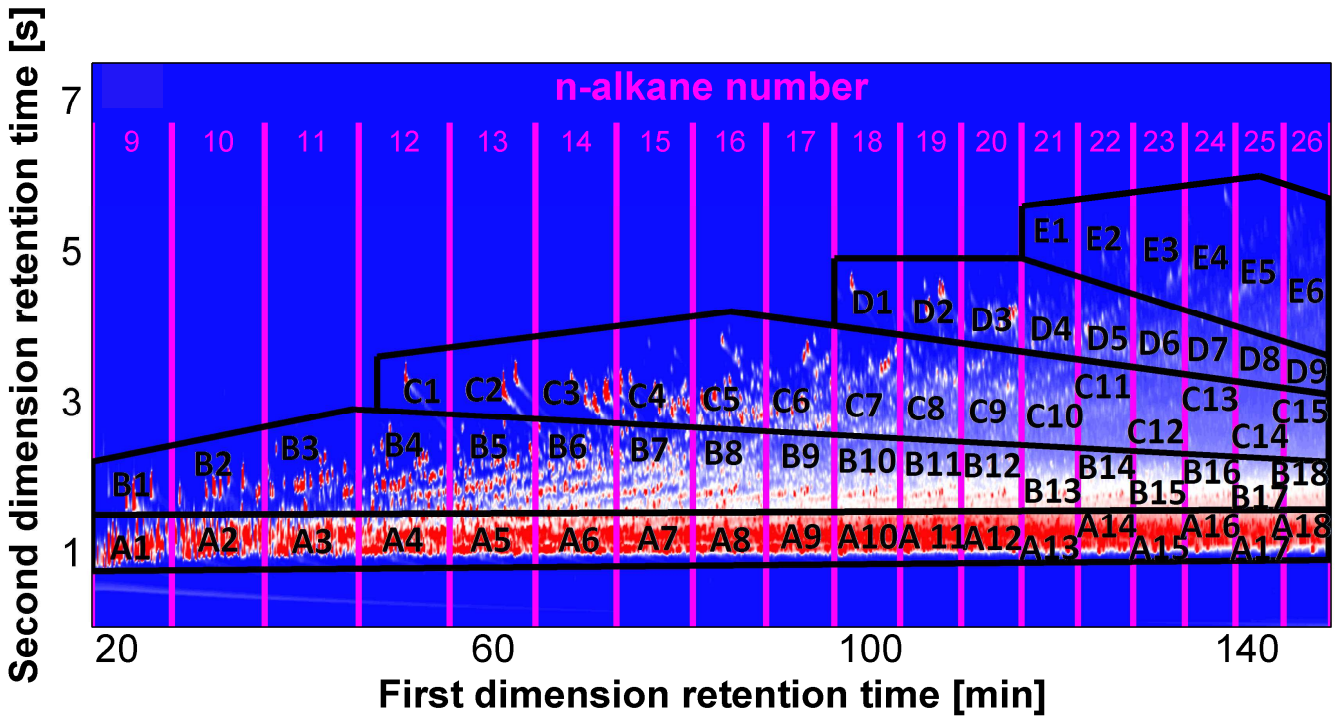

Figure S-5. Names of the pseudocomponents obtained from the GC×GC–FID chromatogram as used in Table S-1, which provides the corresponding chemical names of the approximate structures. Acenaphthene and fluorene (each of which contain 2 aromatic rings and one non-aromatic ring) are included in the 2-ring aromatics group.

Table S-1: Chemical names for the approximate structure of the pseudocomponents obtained from the GC×GC–FID chromatogram (See Fig. S-5 for the pseudocomponent names).

Pseudocomponent name	Chemical name	Number of carbon atoms
A1	*n*-C_9	9
A2	*n*-C_{10}	10
A3	*n*-C_{11}	11
A4	*n*-C_{12}	12
A5	*n*-C_{13}	13
A6	*n*-C_{14}	14
A7	*n*-C_{15}	15
A8	*n*-C_{16}	16
A9	*n*-C_{17}	17
A10	*n*-C_{18}	18
A11	*n*-C_{19}	19
A12	*n*-C_{20}	20
A13	*n*-C_{21}	21
A14	*n*-C_{22}	22
A15	*n*-C_{23}	23
A16	*n*-C_{24}	24
A17	*n*-C_{25}	25
A18	*n*-C_{26}	26
B1	linear ethylbenzene	8

Pseudocomponent name	Chemical name	Number of carbon atoms
B2	linear propylbenzene	9
B3	linear butylbenzene	10
B4	linear pentylbenzene	11
B5	linear hexylbenzene	12
B6	linear heptylbenzene	13
B7	linear octylbenzene	14
B8	linear nonylbenzene	15
B9	linear decylbenzene	16
B10	linear undecylbenzene	17
B11	linear dodecylbenzene	18
B12	linear tridecylbenzene	19
B13	linear tetradecylbenzene	20
B14	linear pentadecylbenzene	21
B15	linear hexadecylbenzene	22
B16	linear heptadecylbenzene	23
B17	linear octadecylbenzene	24
B18	linear nonadecylbenzene	25
C1	naphthalene	10
C2	methylnaphthalene	11
C3	dimethylnaphthalene	12
C4	trimethylnaphthalene	13
C5	tetramethylnaphthalene	14
C6	pentamethylnaphthalene	15
C7	hexamethylnaphthalene	16
C8	heptamethylnaphthalene	17
C9	octamethylnaphthalene	18
C10	(ethyl,heptamethyl)naphthalene	19
C11	(propyl,heptamethyl)naphthalene	20
C12	(butyl,heptamethyl)naphthalene	21
C13	(pentyl,heptamethyl)naphthalene	22
C14	(hexyl,heptamethyl)naphthalene	23
C15	(heptyl,heptamethyl)naphthalene	24
D1	phenanthrene	14
D2	methylphenanthrene	15
D3	dimethylphenanthrene	16
D4	trimethylphenanthrene	17
D5	tetramethylphenanthrene	18
D6	pentamethylphenanthrene	19
D7	hexamethylphenanthrene	20
D8	heptamethylphenanthrene	21
D9	octamethylphenanthrene	22
E1	pyrene	16
E2	methylpyrene	17
E3	dimethylpyrene	18
E4	trimethylpyrene	19
E5	tetramethylpyrene	20
E6	pentamethylpyrene	21

S-8 Definition of pseudocomponents for single carbon number intervals ≥*n*-C_{26} based on simulated distillation data

For chromatographic elution intervals after *n*-C_{26}, we used mass fractions provided by simulated distillation (Section S-5) and we used a classical procedure to define pseudocomponent critical properties and acentric factors. For each carbon number elution interval from C_{26} to C_{108}, correlations were used to estimate the critical properties (Twu)[12] and the acentric factor (Kesler-Lee).[13] In these computations, we assigned molecular weights and specific gravities of carbon number intervals from C_{26} to C_{45} using the values published by Katz and Firoozabadi.[14] This estimation method is often used, bearing in mind that the specific gravities of individual distillation fractions depend slightly on the composition of the oil.[15,16] We followed the procedure of Zuo et al.[16] to extrapolate these data to elution intervals in the C_{46}–C_{108} range:

$$M_i = (14 \cdot N_i - 4) \cdot 10^{-3} \qquad \text{(eq. S-16)}$$

where the molar weight M_i in kg mol^{-1} is estimated from the number of carbon atoms N_i for each carbon number elution interval i after C_{45} ($N_i \geq 46$), and:

$$SG_i = D_1 \cdot \ln(M_i) + D_2 \qquad \text{(eq. S-17)}$$

where SG_i is the specific gravity, and D_1 and D_2 are two fitted constants. We fitted the two constants to the Katz and Firoozabadi values for C_{42} and C_{45}.

S-9 Definition of model composition of MW-1 dead oil, $MC_{1,do}$

The model composition of the MW-1 dead oil, denoted $MC_{1,do}$, was defined based on dead oil analysis. $MC_{1,do}$ is identical to MC_1, except that the mass fractions of CO_2 and C_1–C_6 hydrocarbons have been reassigned to values measured in the dead oil,[7] and the concentrations of all other compounds have been divided by 0.757, taken as the ratio of mass of dead oil to mass of MRF.[7]

S-10 Definitions of model compositions MC_2 and MC_3

Model compositions MC_2 and MC_3 are based on compositional analysis of pre-spill downhole MRF samples by Schlumberger (sample 1.18)[17] and Pencor (sample 53),[18] respectively. These analyses used different gas chromatography devices to quantify mass fractions of N_2, CO_2, and carbon number elution intervals from C_1 to C_{35} (Schlumberger) or to C_{49} (Pencor).

We used the mass fractions reported by these laboratories for N_2, CO_2, and the C_1–C_5 hydrocarbons. The concentrations of all other compounds individually quantified in MW-1 were assumed present in the dead oil fractions of MC_2 and MC_3 at the same concentrations as for MW-1, and their concentrations in MC_2 and MC_3 were therefore normalized according to:

$$m_i(MC_x) = m_i(MC_1) \cdot \frac{m_{C6+}(MC_x)}{m_{C6+}(MC_1)} \qquad \text{(eq. S-18)}$$

where m stands for mass fraction, i for any individual compound $>n$-C_5, x is 2 or 3, and m_{C6+} is the mass fraction of C_{6+} compounds.

We used the simulated distillation data (mass fractions) reported by Schlumberger (MC_2) and Pencor (MC_3) for single carbon number elution intervals up to C_{35} (MC_2) or C_{49} (MC_3). In other words, we used these mass fractions to generate the $<n$-C_{26} pseudocomponents of MC_2 and MC_3 based on the GC×GC–FID chromatogram of MW-1 dead oil. This means that the mass fraction eluting between two consecutive normal alkanes was taken as that measured in the original (Schlumberger or Pencor) sample, whereas the relative contributions of different hydrocarbon compound groups in this mass fraction were assumed the same as found in MW-1.

For MC_2 and MC_3, the assignment of mass fractions for $\geq n$-C_{26} pseudocomponents are described in section S-8. The remaining fraction (C_{36+} or C_{50+}) was separated into single carbon number intervals up to C_{108}, assuming that the relative concentrations were identical to that of MW-1.

MC_2 and MC_3 are very similar to one another, and these model compositions were used to validate the thermodynamic model against laboratory density data (MC_2), gas-liquid equilibrium data (MC_2), and viscosity data (MC_3). The principal difference between MC_1 and the two other model compositions arises from the value of the m_{C6+} fraction (assigned as 0.75 for MC_1 and as 0.65 for MC_2 and MC_3). A minor difference is that MC_1 does not include N_2, therefore MC_1 includes 279 components, whereas MC_2 and MC_3 each include N_2 and therefore each comprise of 280 components.

S-11 Procedure for selection of Henry's law constant values from Sander[19]

To select literature data[19] values of the Henry's law constant for individual compounds, we followed the procedure summarized below. We use the abbreviations "L", "M", "Q", "E", and "?" as defined by Sander,[19] each defined below after their first occurrence. (Note that in order to validate the group-contribution estimation method we retained only a subset of these data, specifically the values taken from literature reviews or measurements.)

- Take the values considered by the author to be the most reliable[19] (category denoted "L" by Sander,[19] from literature reviews), and average them;
- If no value of the "L" type is listed, take the second best type of values ("M", from original publication of a measurement), and average them;
- Otherwise, take all values of any other type that are listed and average them, excluding values with type "Q" (estimate obtained with the quantitative structure property relationship (QSPR)), "E" (estimate), and "?" (the cited reference does not state clearly how the value was obtained).
- As a last resort, take the "Q", "E" and "?" values.

Additionally, we considered only references published from 1950 onward unless no other data were available.

We discarded some obvious outliers among conflicting reported data, as reported below, and we made a few exceptions to the procedure above, also listed below:

- Isopropylbenzene: among the "L" values, we selected the value of $1.2 \cdot 10^{-3}$, and we discarded the value of $7.7 \cdot 10^{-3}$, which is an outlier with respect to the other "L" and "M" values.

- Fluoranthene: the oldest value ($4.5 \cdot 10^{-3}$, two orders of magnitude lower than other reported values) was discarded.

- C_1-naphthalenes, C_2-naphthalenes, C_3-naphthalenes, C_1-phenanthrenes: we took a mean of values for compounds for which an "L" value was reported (obtain a value by structural isomer, average if needed, and then perform an average over all isomers). For example, C_1-naphthalenes corresponds to the grouping of all isomers formed of naphthalene with one methyl substituent. To obtain a value for C_1-naphthalenes, we considered the two isomers for which "L" data were available,[19] 1-methylnaphthalene and 2-methylnaphthalene. The average of "L" values for 1-methylnaphthalene is $2.2 \cdot 10^{-2}$ mol m^{-3} Pa^{-1}, and the only "L" value for 2-methylnaphthalene is $1.8 \cdot 10^{-2}$ mol m^{-3} Pa^{-1}. Hence, the value retained for C_1-naphthalenes is $2.0 \cdot 10^{-2}$ mol m^{-3} Pa^{-1}.

- Normal alkanes from *n*-C_{13} to *n*-C_{20}: considerable discrepancies exist in reported values between different references. We retained data from the only reference that provides data for all of these compounds (Yaws and Yang, 1992). Data for normal alkanes >*n*-C_{20} were discarded. The large discrepancy among available literature data for *n*-C_{13} to *n*-C_{20} normal alkanes[19,20] is not expected to affect predictions of the thermodynamic model for aqueous dissolution extent in the environment, under typical conditions (Figure S-18).

- N_2: the value from the oldest reference was discarded (obtained at a different temperature, 310 K, than the reference temperature chosen, 298.15 K).

S-12 Validation of group-contribution methods for estimation of the chemical properties that are used as inputs for the thermodynamic model

For the thermodynamic model, we used estimated input properties only when literature data were unavailable. However, here we consider the cases where literature measurement data were available, and we compute the corresponding estimated values. We compare the resulting sets of measured and estimated values as a validation exercise for the estimation methods.

Figs. S-6 to S-11 show results of this brief evaluation of the validity of the property-estimation methods. In this series of figures, we compare the literature measurement data to estimates obtained from the selected group-contribution methods, for compounds quantified in MW-1 for which literature measurement data could be found (excluding CO_2). For several methods, the predictions are the least accurate for small compounds (≤*n*-C_5). However, for these small compounds, group-contribution methods were not used for estimating inputs to the thermodynamic model, since literature data were always available.

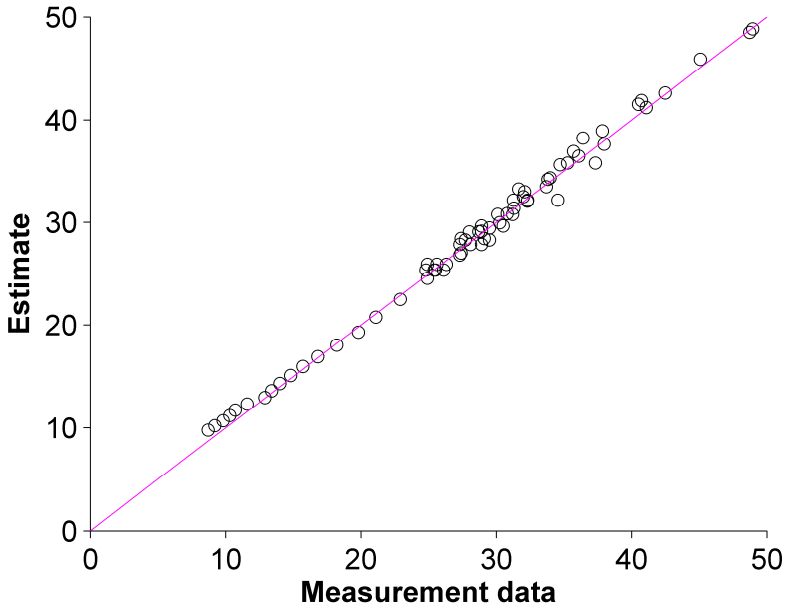

Figure S-6. Comparison of literature measurement data and group-contribution estimates for the critical pressure, in bar. (See Table 1 in main text for references and statistics.)

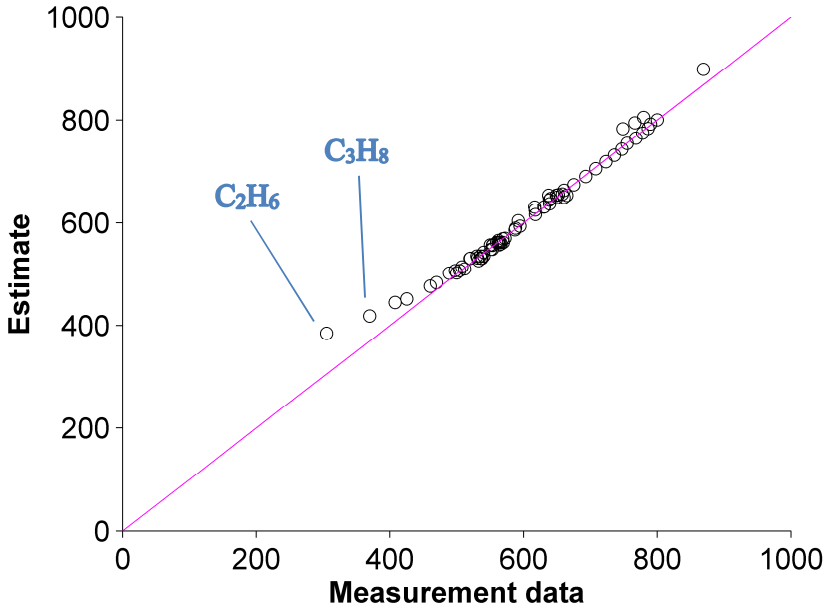

Figure S-7. Comparison of literature measurement data and group-contribution estimates for the critical temperature, in K. (See Table 1 in main text for references and statistics.)

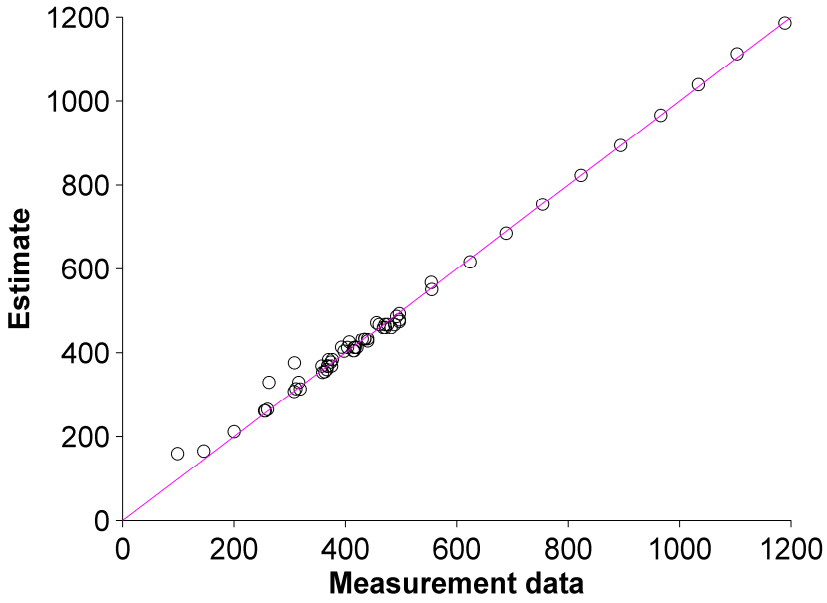

Figure S-8. Comparison of literature measurement data and group-contribution estimates for the critical volume, in $cm^3\ mol^{-1}$. (See Table 1 in main text for references and statistics.)

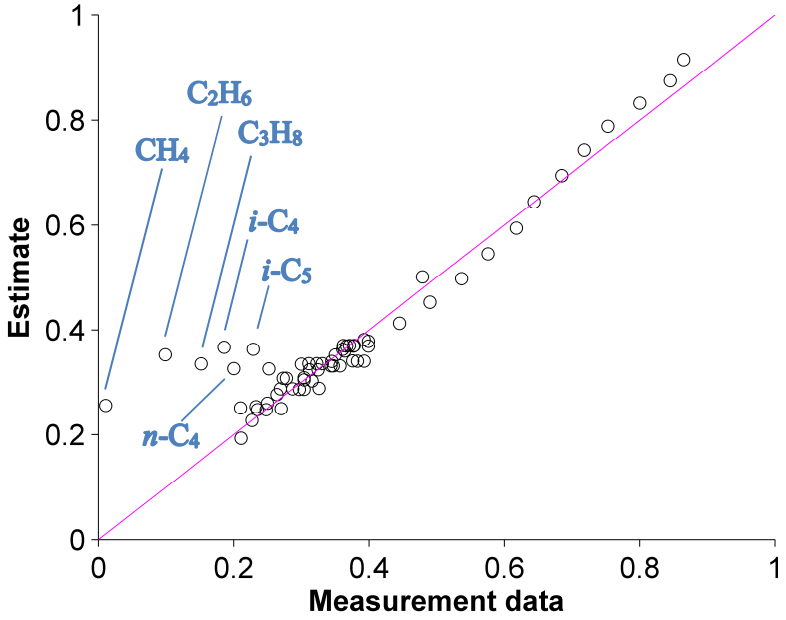

Figure S-9. Comparison of literature measurement data and group-contribution estimates for the acentric factor. (See Table 1 in main text for references and statistics.)

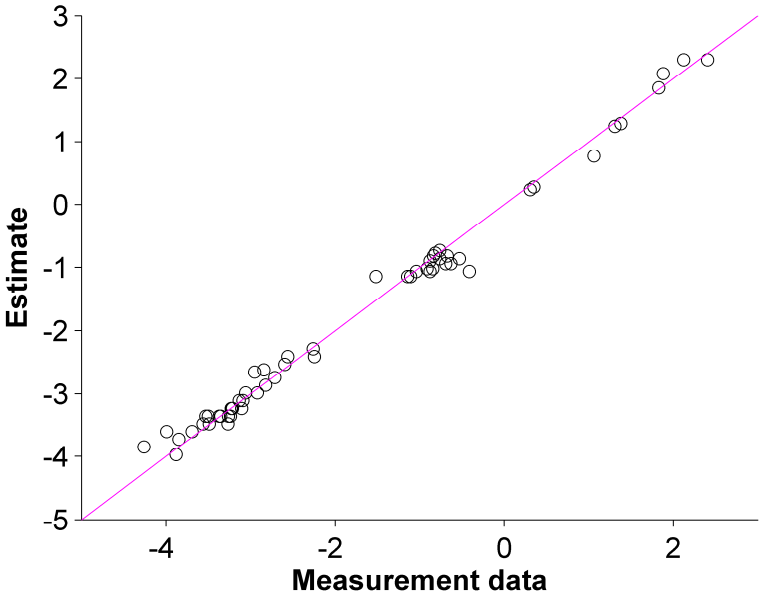

Figure S-10. Comparison of literature measurement data and group-contribution estimates for the (base 10) logarithm of the Henry's law constant, in mol L^{-1} atm^{-1}. (See Table 1 in main text for references and statistics.)

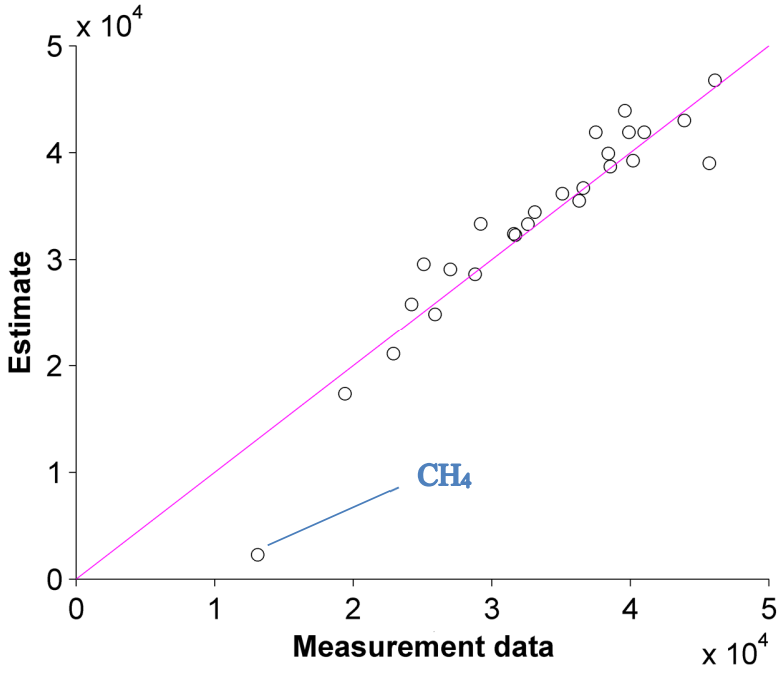

Figure S-11. Comparison of literature measurement data and group-contribution estimates for the negative of the enthalpy of transfer from gas phase to water, in J mol^{-1}. (See Table 1 in main text for references and statistics.)

S-13 Literature measurement data used to derive the correlations of equations 6 and 7

Table S-2. Literature measurement data ($\overline{V}^{L}_{meas,i}$) used to derive the correlation for estimating the partial molar volume at infinite dilution in water (equation 6). The absolute value of the relative error is defined as $\left|\frac{\overline{V}^{L}_{meas,i} - \overline{V}^{L}_{equation\ 6,i}}{\overline{V}^{L}_{meas,i}}\right|$. The McGowan volume, $\overline{V}_{MG}$, is also provided.

Compound	Reference for $\overline{V}^{L}_{meas}$	$\overline{V}^{L}_{meas,i}$ $cm^3\ mol^{-1}$	$\overline{V}^{L}_{equation\ 6,i}$ $cm^3\ mol^{-1}$	$\overline{V}_{MG,i}$ $cm^3\ mol^{-1}$	Absolute relative error
methane	Graziano[21]	34.7	31.6	24.95	9.0%
ethane	Graziano[21]	50.4	47.5	39.04	5.7%
propane	Liu and Ruckenstein[22]	70.7	63.5	53.13	10.2%
i-C_4	Liu and Ruckenstein[22]	81.3	79.4	67.22	2.3%
n-C_4	Liu and Ruckenstein[22]	76.6	79.4	67.22	3.7%
n-C_5	Liu and Ruckenstein[22]	92.3	95.4	81.31	3.3%
CO_2	King[23]	32	35.1	28.09	9.8%
cyclopentane	Liu and Ruckenstein[22]	84.5	83.1	70.45	1.7%
2,3-dimethylbutane	Liu and Ruckenstein[22]	106.8	111.3	95.40	4.2%
n-C_6	Liu and Ruckenstein[22]	110	111.3	95.40	1.2%
benzene	Liu and Ruckenstein[22]	82.5	84.4	71.64	2.3%
cyclohexane	Liu and Ruckenstein[22]	98.8	99.0	84.54	0.2%
n-C_7	Liu and Ruckenstein[22]	129.4	127.3	109.49	1.7%
toluene	Liu and Ruckenstein[22]	97.7	100.4	85.73	2.7%
n-C_8	Liu and Ruckenstein[22]	145.2	143.2	123.58	1.4%
ethylbenzene	Liu and Ruckenstein[22]	111.1	116.3	99.82	4.7%
n-C_{10}	Liu and Ruckenstein[22]	176.8	175.1	151.76	1.0%
n-C_{12}	Liu and Ruckenstein[22]	209.5	207.0	179.94	1.2%

K_{salt} values measured in seawater or NaCl solutions usually agree with one another, within experimental errors.[24] Therefore, although we preferred data for seawater or artificial seawater whenever available, we included values obtained with NaCl when this was the only information available. The salts used to obtain the experimental values are listed in Table S-3.

Table S-3. Literature measurement data ($K_{salt,meas,i}$) used to derive the correlation for estimating the Setschenow constant (equation 7). The absolute value of the relative error is defined as $\left|\frac{K_{salt,meas,i} - K_{salt,equation\ 7,i}}{K_{salt,meas,i}}\right|$.

Compound	Reference for $K_{salt,meas,i}$	Salt	$K_{salt,meas,i}$ L mol^{-1}	$K_{salt,equation\ 7,i}$ L mol^{-1}	Absolute relative error
methane	Ni and Yalkowsky[25]	NaCl	0.127	0.159	25.3%
ethane	Ni and Yalkowsky[25]	NaCl	0.162	0.184	13.7%
propane	Ni and Yalkowsky[25]	NaCl	0.194	0.222	14.5%
n-C_4	Ni and Yalkowsky[25]	NaCl	0.217	0.220	1.3%
n-C_5	Xie et al.[26]	"artificial, NaCl"	0.221	0.245	10.8%
CO_2	Weiss[27]	seawater	0.132	0.114	13.9%
cyclopentane	Xie et al.[26]	NaCl	0.182	0.226	24.1%
n-C_6	Xie et al.[26]	NaCl	0.276	0.276	0.2%
methylcyclopentane	Xie et al.[26]	"artificial, NaCl"	0.273	0.248	9.3%
benzene	Schwarzenbach et al.[24]	seawater	0.200	0.209	4.7%
cyclohexane	Xie et al.[26]	NaCl	0.277	0.247	10.9%
methylcyclohexane	Xie et al.[26]	NaCl	0.274	0.273	0.2%
toluene	Schwarzenbach et al.[24]	seawater	0.240	0.233	2.9%
ethylbenzene	Schwarzenbach et al.[24]	seawater	0.290	0.252	13.2%
p/m-xylenes	Schwarzenbach et al.[24]	seawater	0.295	0.266	9.7%
o-xylene	Schwarzenbach et al.[24]	seawater	0.300	0.266	11.2%
isopropylbenzene	Xie et al.[26]	artificial seawater	0.316	0.292	7.5%
1,3,5-trimethylbenzene	Xie et al.[26]	artificial seawater	0.318	0.292	8.1%
1,2,4-trimethylbenzene	Xie et al.[26]	artificial seawater	0.293	0.292	0.3%
sec-butylbenzene	Xie et al.[26]	artificial seawater	0.288	0.318	10.4%
1,2,3-trimethylbenzene	Xie et al.[26]	artificial seawater	0.321	0.344	7.2%
n-butylbenzene	Xie et al.[26]	artificial seawater	0.375	0.318	15.2%
naphthalene	Schwarzenbach et al.[24]	seawater	0.280	0.264	5.6%
fluorene	Xie et al.[26]	NaCl	0.267	0.299	12.0%
phenanthrene	Schwarzenbach et al.[24]	seawater	0.300	0.314	4.7%
fluoranthene	Xie et al.[26]	NaCl	0.339	0.323	4.7%
pyrene	Schwarzenbach et al.[24]	seawater	0.300	0.323	7.6%
benz[a]anthracene	Xie et al.[26]	NaCl	0.354	0.364	2.7%
chrysene	Xie et al.[26]	NaCl	0.336	0.364	8.2%

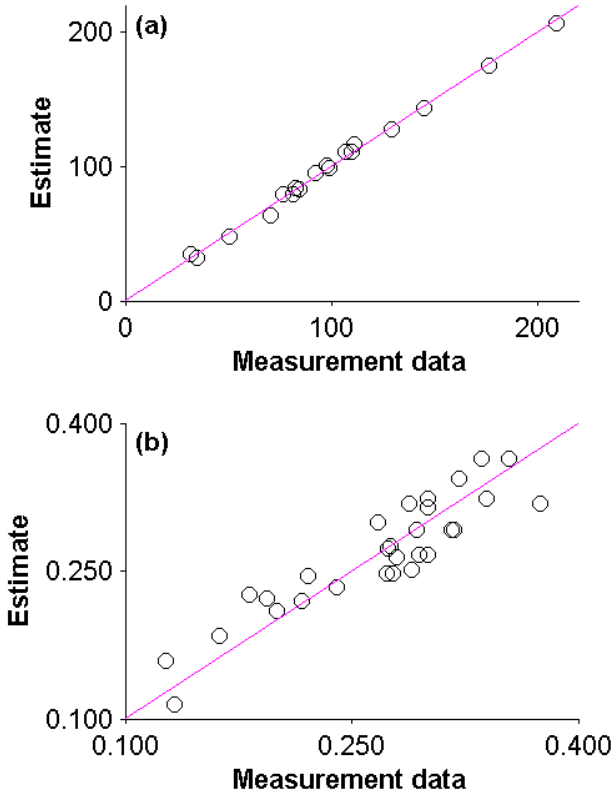

Figure S-12. (a) Comparison of measured $\bar{v}_i^L$ data (from literature) with estimates according to equation 6, and (b) comparison of measured K_{salt} data (literature) with estimates according to equation 7 (see Tables S-2 and S-3 for the lists of compounds and the numerical values). The 1:1 line is shown in pink.

S-14 Methodological differences between the thermodynamic model of the present study and the Zick model

In this section we specifically discuss the differences between the gas-liquid equilibrium calculations of our thermodynamic model and those of the Zick model. The Zick model relies on the same EOS as used by us (1978 Peng-Robinson EOS). The thermodynamic model of the present study assumes that, based on the detailed compositional information available (~280 components), valid predictions can be obtained without requiring any tuning of either the EOS parameters or the modeled composition. In contrast, the model developed by Aaron A. Zick employed only 11 components and was tuned to match approximately 1000 individual measurements. EOS tuning is a frequently used procedure that usually implies careful modification of the values of some properties of the components (e.g. binary interaction parameters) in order to improve the correspondence between EOS predictions and laboratory data acquired with reservoir fluid samples. The detailed tuning procedure can be found in his report,[6] we will only mention here that the Zick model tuning also included the adjustment of the composition of the sample 1.18 of Schlumberger. However, MC_2 (as defined in the current study) is based on the untuned composition. (Using the tuned composition instead was found to provide less satisfactory predictions with our

thermodynamic model.) The final component properties that Zick obtained are listed in Tables S-4 and S-5.

Three additional differences between the Zick model and our model should be mentioned:

(1) Volume translation. In the Zick model, a fixed volume shift parameter, *VS*, was assigned for each component as listed in Table S-4. *VS* is related to the volume translation parameter, *c*, through:

$$c_i = VS_i \cdot 0.07780 \cdot R \cdot \frac{T_{c,i}}{P_{c,i}} \qquad \text{(eq. S-19)}$$

$$c = \sum z_i \cdot c_i \qquad \text{(eq. S-20)}$$

where z_i is the mole fraction of component i in the phase of interest, $T_{c,i}$ is the critical temperature of component i, $P_{c,i}$ the critical pressure of component i, and R the molar gas constant.

By contrast, in the thermodynamic model of the present study, we used the Lin-Duan method to estimate the volume translation parameter from critical properties and acentric factors.[28]

(2) Viscosity. Zick used the Lohrenz-Bray-Clark viscosity model,[29] whereas we preferred the Pedersen et al. viscosity model, which has better predictive capabilities without tuning.[15] We modified slightly the Pedersen et al. procedure to use our (volume-translated) EOS for estimating the reference compound (methane) density; Lin and Duan obtained a mean absolute error of 0.61% for the saturated liquid density of methane (in a reduced temperature range of 0.483–0.997).[28] We did not include the modification of the Pedersen et al. procedure for heavy oils,[15] because our oil was relatively light and also because the original model proved to provide more robust predictions.

(3) Binary interaction parameters. Finally, the Zick model used temperature-independent, constant binary interaction parameters (Table S-5), whereas in the present study we estimated temperature-dependent binary interaction parameters from a group-contribution method.[30]

All predictions from the Zick model presented here were obtained by use of our own Matlab[1] implementation of his model. Except for the differences mentioned above, our implementation of the Zick model corresponds to the same algorithms as our thermodynamic model applied to MC_2 and MC_3. The values obtained with our Matlab[1] implementation for the Zick model compared favorably with the values originally obtained by Zick with his EOS software PhaseComp (based on figures in his report[6] and personal communication on 26th May 2015).

To validate the implementation of our model, we compared results for EOS gas-liquid equilibrium calculations (Section S-3) with results given by the software provided as supplementary material to the book by Michelsen and Mollerup,[4] available at: http://www.tie-tech.com/products/publications/more.php?id=32_0_1_0_M13 (accessed on 29th May 2015). Based on the agreement found between these two implementations, we conclude that our computational procedure has a correct technical implementation. (The same procedure is used for gas-liquid equilibrium calculations (Section S-3) in both our thermodynamic model and the Zick model.)

Table S-4: List of the properties of the 11 components of the Zick model.[6] These properties include the molar weight, M; the critical temperature, T_c; the critical pressure, P_c; the acentric factor, ω; the volume shift parameter, VS; the critical volume, V_c; the mass fraction in Schlumberger sample 1.18, $MC_{z,2}$; and the mass fraction in Pencor sample 53, $MC_{z,3}$.[6]

Component	M (g/mol)	T_c (K)	P_c (MPa)	ω (-)	VS (-)	V_c ($cm^3\ mol^{-1}$)	$MC_{z,2}$ (-)	$MC_{z,3}$ (-)
N_2	28.014	126.20	3.3980	0.037	-0.16758	90.10	0.00175562	0.00237483
CO_2	44.01	304.12	7.3740	0.225	0.00191	94.07	0.00813986	0.00771591
C_1	16.043	190.56	4.5990	0.011	-0.14996	98.60	0.1926728	0.2003477
C_2	30.07	305.32	4.8720	0.099	-0.0628	145.50	0.0398621	0.03681465
C_3	44.097	369.83	4.2480	0.152	-0.06381	200.00	0.04141159	0.03845829
C_4-C_5	63.37	437.51	3.5949	0.21328	-0.05005	273.70	0.06351786	0.06161619
C_6-C_7	89.779	523.09	3.0992	0.27691	0.00117	371.30	0.05626886	0.05887051
C_8-C_9	113.271	578.88	2.7419	0.33414	0.0283	463.30	0.0757595	0.07900799
C_{10}-C_{12}	151.237	650.89	2.3257	0.42755	0.05886	612.92	0.08579121	0.0835788
C_{13}-C_{19}	215.517	739.12	1.8630	0.57931	0.0893	857.67	0.1502443	0.1527663
C_{20+}	441.107	892.62	1.2566	1.09027	0.00389	1669.51	0.2845762	0.2784489

Table S-5: Binary interaction parameter values for the Zick model.[6]

	N_2	CO_2	C_1	C_2	C_3	C_4-C_5	C_6-C_7	C_8-C_9	C_{10}-C_{12}	C_{13}-C_{19}	C_{20+}
N_2	0	0	0.025	0.01	0.09	0.09943	0.11	0.11	0.11	0.11	0.09453
CO_2	0	0	0.105	0.13	0.125	0.11587	0.115	0.115	0.115	0.115	0.09962
C_1	0.025	0.105	0	0.00097	0.00319	0.00689	0.01123	0.01478	0.01981	0.0269	0.06074
C_2	0.01	0.13	0.00097	0	0	0	0	0	0	0	0.02106
C_3	0.09	0.125	0.00319	0	0	0	0	0	0	0	0.02106
C_4-C_5	0.09943	0.11587	0.00689	0	0	0	0	0	0	0	0.02106
C_6-C_7	0.11	0.115	0.01123	0	0	0	0	0	0	0	0.02106
C_8-C_9	0.11	0.115	0.01478	0	0	0	0	0	0	0	0.02106
C_{10}-C_{12}	0.11	0.115	0.01981	0	0	0	0	0	0	0	0.02106
C_{13}-C_{19}	0.11	0.115	0.0269	0	0	0	0	0	0	0	0.02106
C_{20+}	0.09453	0.09962	0.06074	0.02106	0.02106	0.02106	0.02106	0.02106	0.02106	0.02106	0

S-15 Validation of our thermodynamic model with laboratory data and comparison with the Zick model

To validate our thermodynamic model, we made comparisons with measured laboratory data and also with predictions of the Zick model. We considered three different types of data: (a) the density of the single-phase fluid at high pressures; (b) the volume fraction of liquid at lower pressures; and (c) the predicted viscosities of the single-phase fluid or liquid phase. Each of these tests is described in turn below.

(a) Density of the single-phase fluid.

Both our thermodynamic model and the Zick model perform well at predicting the density of the single-phase fluid, with maximum deviations of 6 and 10 kg m^{-3}, respectively, or ~1% error (Table S-6). Our model slightly underpredicts the bubble point pressure at 390.4 K, whereas the Zick model slightly overpredicts the bubble point pressure (Table S-6).

To evaluate model prediction skill for fluid density, we selected laboratory data from Schlumberger,[17] obtained with their sample 1.18 at 243°F (390.4 K). Therefore, for the purpose of evaluating model predictive capabilities for fluid density, the model composition MC_2 was used for our thermodynamic model and the model composition $MC_{z,2}$ (as tuned by Zick) was used for the Zick model. As discussed by Zick,[6] there is some disagreement among the available laboratory data regarding the phase envelope, with incompatible dew points and bubble points obtained by Pencor[18] and Schlumberger,[17] respectively, in the 310–390 K temperature range (and pressures around 40 MPa). Zick concludes that this inconsistency cannot be explained, and he managed to match his EOS predictions to the experimental

bubble points in the 310–390 K temperature range and also to the experimental dew points at lower temperatures, by tuning both the component properties and the model fluid composition $MC_{z,2}$. However, we bring attention to the fact that some uncertainty remains regarding the real behavior of the MRF at pressures of 40 MPa and temperatures <310 K,[6] which are conditions that exceed substantially the pressures and temperatures encountered during the release in the Gulf of Mexico at ~1524 m depth (~15 MPa and ~278 K).

Table S-6: Single-phase fluid density at 243°F (390.4 K).

Pressure (psia)	**Pressure (MPa)**	**Density from laboratory[17,a] (kg m^{-3})**	**Density according to our thermodynamic model, with model composition MC_2 (kg m^{-3})**	**Density according to the Zick model, with model composition $MC_{z,2}$ (kg m^{-3})**
15015	103.5	610–613	613	620
14015	96.6	601–607	607	614
13015	89.7	598–598	600	608
11871	81.8	590–591	591	600
10015	69.1	575–576	575	584
9015	62.2	562–568	565	574
8015	55.3	555–556	553	563
7015	48.4	543–544	539	550
6370	43.9	535–536	529	two phases: 434 and 559
6348	43.8	535–536	529	two phases: 431 and 561

[a] The two density values reported by Schlumberger were described as follows in their report: "liquid densities were measured using two methods at 15000 psia, 14000 psia, 10000 psia, and 9000 psia at 243°F, known volume displacement into pre-weighted cylinder and a direct read from an Anton Parr densitometer. Densities at all other points are calculated from the values at 10000 psia."[17]

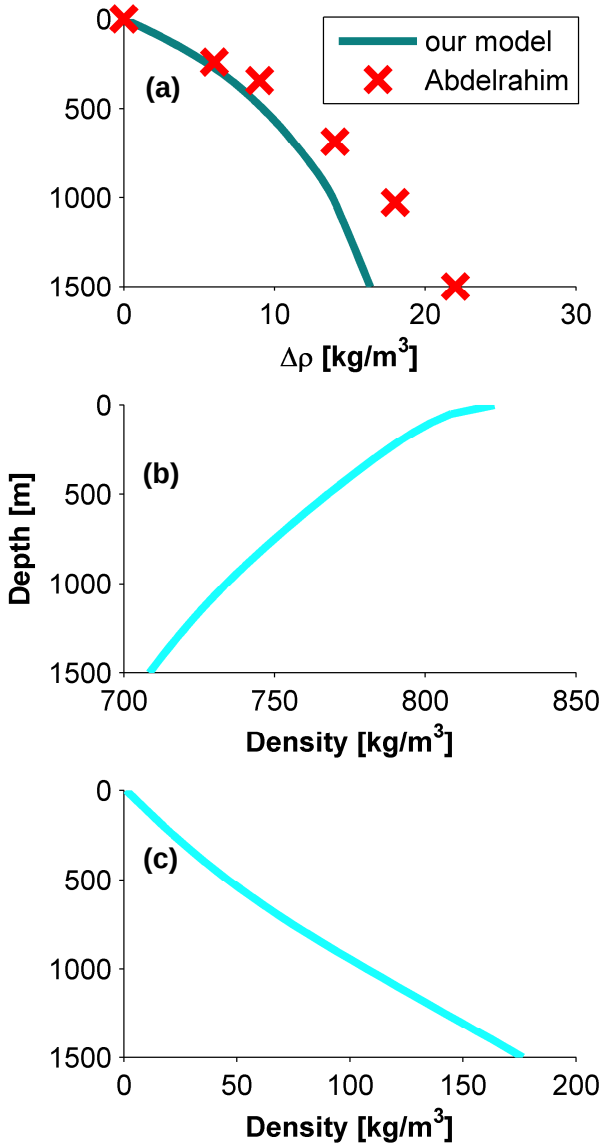

Figure S-13. (a) Predicted and measured density change, $\Delta\rho$, as a function of depth for Macondo dead oil, where $\Delta\rho = \rho(P,T) - \rho(P_{surface},T_{surface})$; (b) predicted live oil density as a function of depth; and (c) the predicted density as a function of depth, for the gas phase at equilibrium with the live oil. The measured pressure and temperature conditions as a function of depth were interpolated from the values reported by Abdelrahim.[31] The blue line shows the predictions of our thermodynamic model for model compositions MC_1 (light blue) and $MC_{1,do}$ (dark blue), whereas the red crosses are laboratory measurements by Abdelrahim. Abdelrahim used a different sample of *Deepwater Horizon* dead oil, which has a reported density at surface conditions (~847 kg m^{-3}) that differs slightly from the density of MW-1 dead oil (820 kg m^{-3}). Values of $\Delta\rho$ from Abdelrahim were obtained from his Figure 32. The reported density predictions shown above assume that the (dead or live) oil composition has not been altered by fractionation processes such as water-washing (aqueous dissolution) and evaporation. Therefore these results should not be construed to convey the predicted fluid densities of oil droplets or gas bubbles ascending the water column after emission from the Macondo well.

(b) Percent of liquid for the two-phase region.

At 243°F (390.4 K), spontaneous separation of the MRF into a liquid phase and a gas phase is reproduced within 16% at pressures ≤50 MPa by both our thermodynamic model and the Zick model (Table S-7).

Table S-7: Predicted and measured volume fraction[a] of liquid for the two-phase region at 243°F (390.4 K).[b]

Pressure (psia)	Pressure (MPa)	Experimental liquid volume fraction[17] (-)	Liquid volume fraction according to our thermodynamic model, with model composition MC_2 (-)	Liquid volume fraction according to the Zick model, with model composition $MC_{z,2}$ (-)
5039	34.7	0.608	0.674	0.606
4537	31.3	0.579	0.602	0.563
4037	27.8	0.541	0.537	0.518
3536	24.4	0.496	0.473	0.468
3025	20.9	0.445	0.408	0.411
2530	17.4	0.386	0.343	0.349
2027	14.0	0.315	0.273	0.281
1525	10.5	0.239	0.201	0.208
1098	7.6	0.164	0.140	0.144

[a] E.g. a liquid volume fraction value of "0.99" means 99% liquid and 1% gas, by volume. [b] Values in between the bubble point pressure (6348 psia) and 5039 psia were not considered here, since large discrepancies between laboratory data from Pencor (dew point) and Schlumberger (bubble point) were noticed in this pressure range.[6] Therefore it was chosen to perform validation only based on the unambiguous data reported for the 5039 to 1098 psia range.

For conditions from emission depth (~15 MPa and ~278 K) to sea surface (~0.1 MPa and ~300 K), our thermodynamic model and the Zick model are in good agreement with each other. However, at substantially higher pressures (~40 MPa), our model predicts a bubble point <310 K, whereas the Zick model predicts a dew point in agreement with available experimental data (Figs. S-14 and S-15). Larger discrepancies in the two models would arise for water depths of >2500 m.

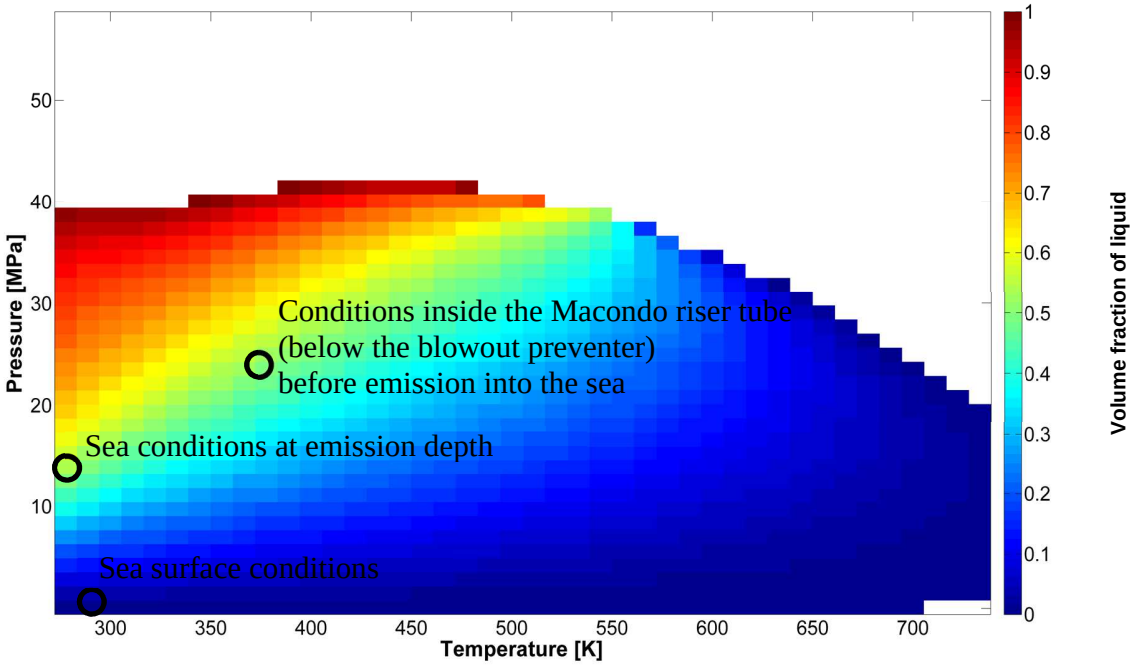

Figure S-14. Phase envelope of MRF as predicted by our model using model composition MC_3. The colored pixels are predicted to be within the two-phase region, where the color shade represents the volume fraction of liquid, ranging from 0 (100% gas) to 1 (100% liquid). The single-phase region is displayed in white.

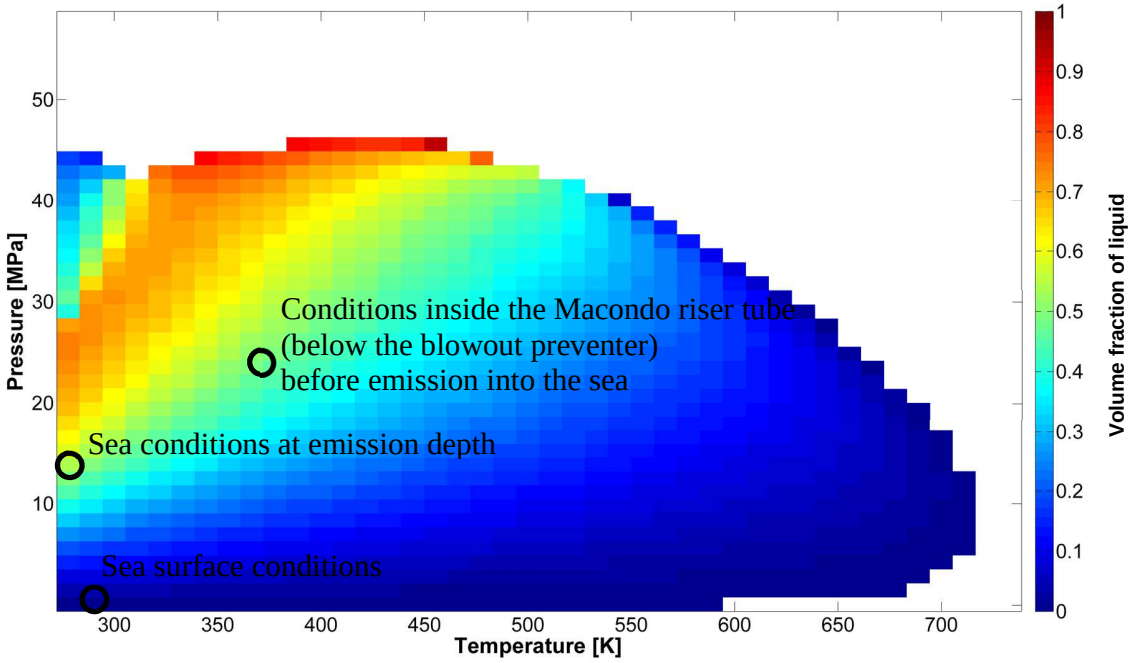

Figure S-15. Phase envelope of MRF as predicted by the Zick model using model composition $MC_{z,3}$. The colored pixels are predicted to be within the two-phase region, where the color shade represents the volume fraction of liquid, ranging from 0 (100% gas) to 1 (100% liquid). The single-phase region is displayed in white.

(c) Viscosity for the single-phase fluid or liquid phase.

High-pressure experimental viscosity data were reported previously for Pencor sample 53,[18] and therefore the corresponding model compositions MC_3 and $MC_{z,3}$ were used. First, it should be explained how viscosity data were obtained (according to a usual procedure among specialists, with which some readers may be unfamiliar). The test begins at high pressure with a single-phase fluid. The temperature is maintained constant, and the pressure is decreased in a step-wise fashion. At each step, if the fluid is single phase, its viscosity is measured; if there are two phases present, the gas phase is discarded, and the viscosity is measured for the liquid phase; then the experiment continues with the liquid phase. Petroleum engineers call this procedure, where the generated gas phase is discarded at each step, a *differential liberation experiment*. This same procedure is also what was modeled with our thermodynamic model and with the Zick model. However, errors in phase partitioning predictions, especially when near a dew point, will tend to alter the quality of the viscosity predictions (which will be based on an inaccurate composition of the liquid phase), independently of the predictive abilities of the chosen viscosity model. This explains why poorer predictions arise for our model at 40°F (277.6 K) and <46 MPa for the two-phase region (Fig. S-16), where our thermodynamic model fails to correctly predict the experimental dew point. For the pressure and temperature conditions under which our model predicts the gas-liquid partitioning correctly, the predicted viscosities of our model and the Zick model exhibit similar extent of agreement with the laboratory data (Figs. S-16 and S-17). We interpret that the predictive viscosity model used by us is representative of the viscosity of the Macondo fluids to within a factor of 2 to 10. We infer that predictions of viscosity at deep-water conditions (<2500 m depth) by our model would be similar to

that of the Zick model, because the gas-liquid partitioning predicted by our model and the Zick model are very similar at these conditions (Figs. S-14 and S-15).

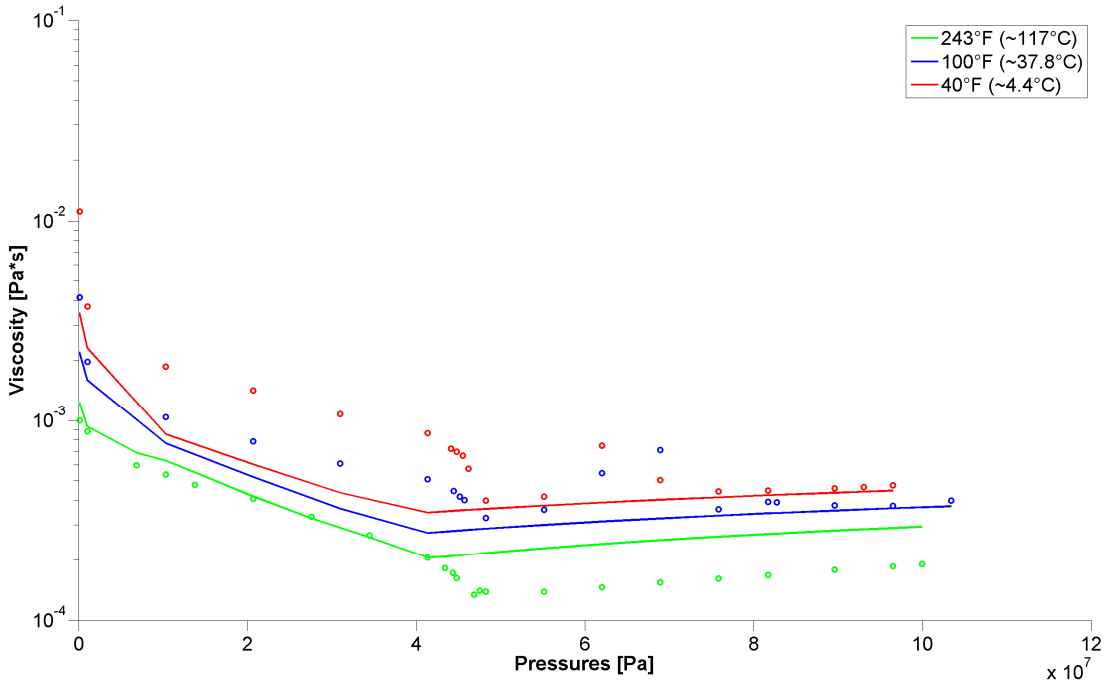

Figure S-16. Comparison of measured (circles) and predicted (lines) viscosities of the single-phase fluid or liquid phase. Predictions are shown for our thermodynamic model using model composition MC_3 and the Pedersen et al. viscosity model.

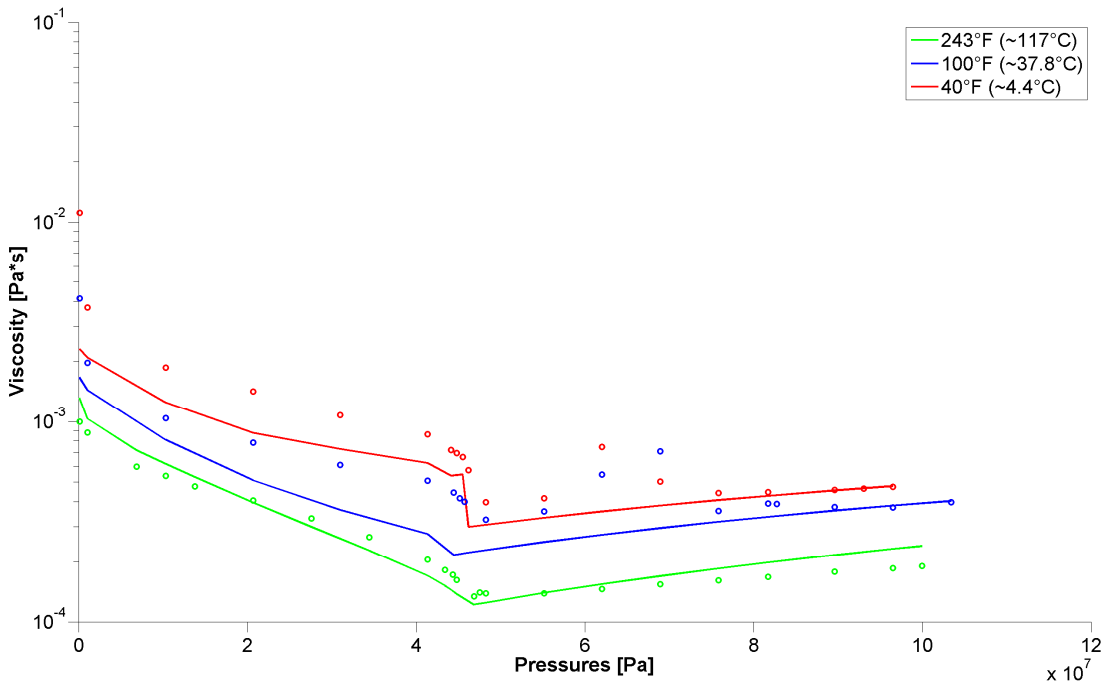

Figure S-17. Comparison of measured (circles) and predicted (lines) viscosities of the single-phase fluid or liquid phase. Predictions are shown for the Zick model using model composition $MC_{z,3}$ and the Lohrenz-Bray-Clark viscosity model.

S-16 Model domain of validity (extended discussion)

The thermodynamic model presented here is not validated for brines under oil reservoir conditions, because: (i) the equation of state calculations neglect the influence of water[32,33] on the fugacities in the hydrocarbon-rich phase(s), and this approximation will become increasingly inappropriate as pressure and temperature are raised; (ii) we are unaware of datasets used to validate the combined adjustment of Henry's law constant to oil reservoir pressure and temperature conditions; (iii) the adjustment for the effect of salt is valid up to a concentration of 2–5 M,[34] whereas salt concentrations in reservoir brines can be much higher.[5]

S-17 Predicted density of Macondo dead oil and live oil as a function of dissolution and evaporation extent

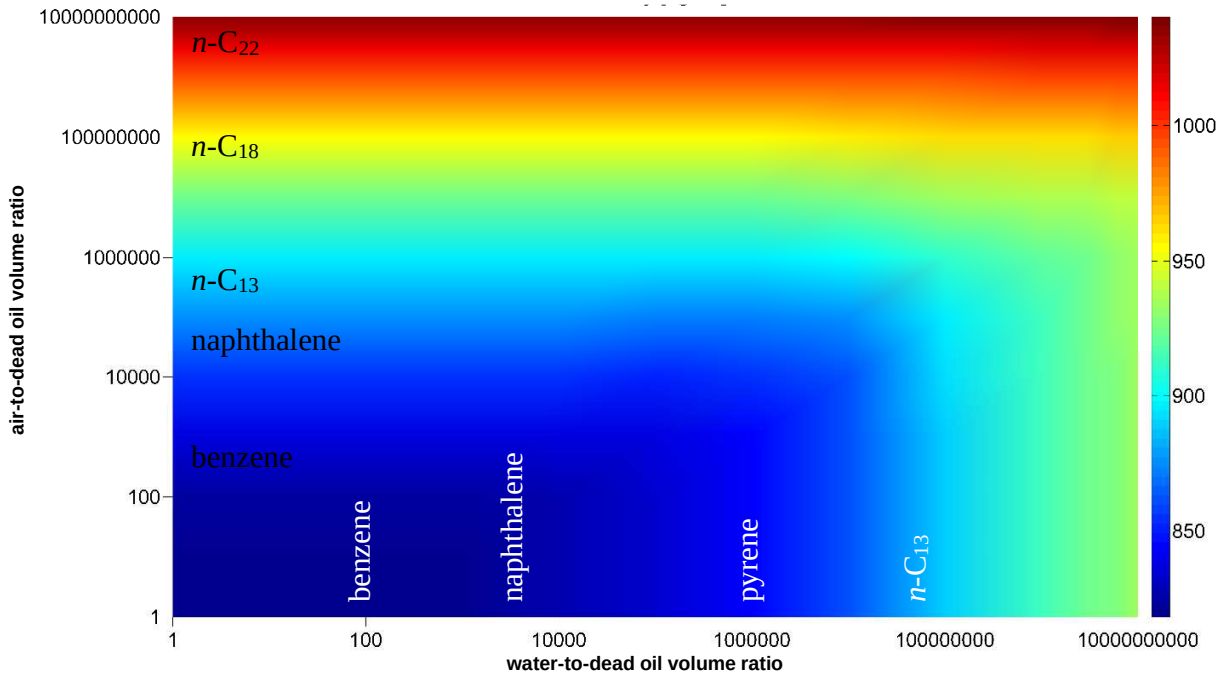

Figure S-18. Density (kg m^{-3}) of $MC_{1,do}$ as a function of extent of dissolution and evaporation (expressed as water-to-dead oil ratio and air-to-dead oil ratio, by volume), as predicted by our thermodynamic model at 101325 Pa (1 atm) and 25°C. Labeled compound names indicate the location on the plot where 50% depletion from the oil by evaporation (black font) or dissolution (white font) would be expected, according to equilibrium partitioning calculations.

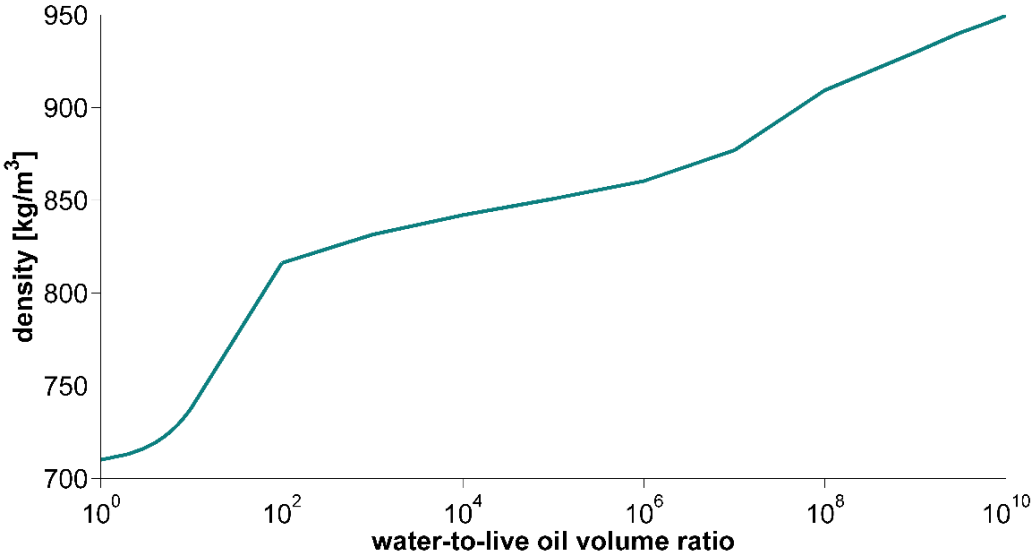

Figure S-19. Predicted density (kg m^{-3}) of MC_1 liquid phase at emission depth (15.5 MPa and 4.3 °C) as a function of dissolution extent (expressed as water-to-live oil volume ratio).

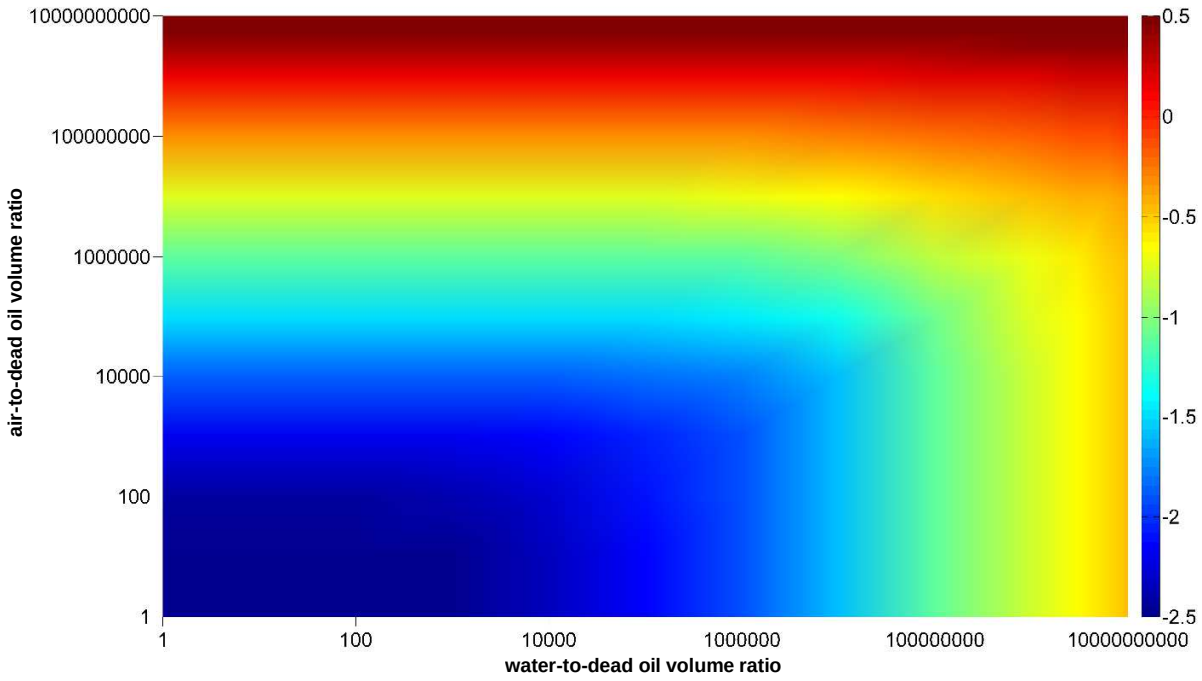

Figure S-20. Base 10 logarithm of the viscosity (Pa s) of $MC_{1,do}$ as a function of extent of dissolution and evaporation (expressed as water-to-dead oil ratio and air-to-dead oil ratio, by volume), as predicted by our thermodynamic model at 101325 Pa and 25°C.

References

(1) *Matlab*; The MathWorks Inc.: Natick, 2014.

(2) Nabi, D.; Gros, J.; Dimitriou-Christidis, P.; Arey, J. S. Mapping environmental partitioning properties of nonpolar complex mixtures by use of GC × GC. *Environ. Sci. Technol.* **2014**, *48*, 6814–6826.

(3) Peng, D.-Y.; Robinson, D. B. A new two-constant equation of state. *Ind. Eng. Chem. Fundam.* **1976**, *15*, 59–64.

(4) Michelsen, M. L.; Mollerup, J. M. *Thermodynamic Models: Fundamentals & Computational Aspects*; 2nd ed.; Tie-Line Publications: Holte, 2007.

(5) McCain, W. D. Jr. *The Properties of Petroleum Fluids*; 2nd ed.; PennWell: Tulsa, 1990.

(6) Zick, A. A. *Equation-of-state fluid characterization and analysis of the Macondo reservoir fluids*; Expert report prepared on behalf of the United States TREX-011490R; 2013, (evidence in the *United States of America v. BP Exploration & Production, Inc., et al.* case).

(7) Reddy, C. M.; Arey, J. S.; Seewald, J. S.; Sylva, S. P.; Lemkau, K. L.; Nelson, R. K.; Carmichael, C. A.; McIntyre, C. P.; Fenwick, J.; Ventura, G. T.; Mooy, B. A. S. V.; Camilli, R. Composition and fate of gas and oil released to the water column during the *Deepwater Horizon* oil spill. *Proc. Natl. Acad. Sci.* **2012**, *109*, 20229–20234.

(8) Samanipour, S.; Dimitriou-Christidis, P.; Gros, J.; Grange, A.; Arey, J. S. Analyte quantification with comprehensive two-dimensional gas chromatography: Assessment of methods for baseline correction, peak delineation, and matrix effect elimination for real samples. *J. Chromatogr. A* **2015**, *1375*, 123–139.

(9) Gros, J.; Reddy, C. M.; Aeppli, C.; Nelson, R. K.; Carmichael, C. A.; Arey, J. S. Resolving biodegradation patterns of persistent saturated hydrocarbons in weathered oil samples from the *Deepwater Horizon* disaster. *Environ. Sci. Technol*. **2014**, *48*, 1628–1637.
(10) Reichenbach, S. E.; Ni, M.; Zhang, D.; Ledford Jr., E. B. Image background removal in comprehensive two-dimensional gas chromatography. *J. Chromatogr. A* **2003**, *985*, 47–56.
(11) Reichenbach, S. E.; Ni, M.; Kottapalli, V.; Visvanathan, A. Information technologies for comprehensive two-dimensional gas chromatography. *Chemom. Intell. Lab. Syst.* **2004**, *71*, 107–120.
(12) Twu, C. H. An internally consistent correlation for predicting the critical properties and molecular weights of petroleum and coal-tar liquids. *Fluid Phase Equilibria* **1984**, *16*, 137–150.
(13) Chen, D. H.; Dinivahi, M. V.; Jeng, C. Y. New acentric factor correlation based on the Antoine equation. *Ind. Eng. Chem. Res.* **1993**, *32*, 241–244.
(14) Katz, D. L.; Firoozabadi, A. Predicting phase behavior of condensate/crude-oil systems using methane interaction coefficients. *J. Pet. Technol.* **1978**, *30*, 1649–1655.
(15) Pedersen, K. S.; Christensen, P. L.; Shaikh, J. A. *Phase Behavior of Petroleum Reservoir Fluids*; 2nd ed.; CRC Press: Boca Raton, 2014.
(16) Zuo, J. Y.; Zhang, D.; Dubost, F.; Dong, C.; Mullins, O. C.; O'Keefe, M.; Betancourt, S. S. EOS-based downhole fluid characterization. In *SPE 114702*; Society of Petroleum Engineers, 2008.
(17) Mathews, S. G. *Fluid analysis on Macondo samples*; Reservoir sample analysis report TREX-011575; Schlumberger: Houston, 2010; p. 50, (evidence in the *United States of America v. BP Exploration & Production, Inc., et al.* case).
(18) LeBlanc, J. *Volatile oil reservoir fluid study for BP*; TREX-130815; Pencor: Broussard, 2010, (evidence in the *United States of America v. BP Exploration & Production, Inc., et al.* case).
(19) Sander, R. Compilation of Henry's law constants, version 3.99. *Atmos Chem Phys Discuss* **2014**, *14*, 29615–30521.
(20) Ferguson, A. L.; Debenedetti, P. G.; Panagiotopoulos, A. Z. Solubility and molecular conformations of *n*-alkane chains in water. *J. Phys. Chem. B* **2009**, *113*, 6405–6414.
(21) Graziano, G. Partial molar volume of *n*-alcohols at infinite dilution in water calculated by means of scaled particle theory. *J. Chem. Phys.* **2006**, *124*, 134507.
(22) Liu, H.; Ruckenstein, E. Aggregation of hydrocarbons in dilute aqueous solutions. *J. Phys. Chem. B* **1998**, *102*, 1005–1012.
(23) King, M. B. *Phase Equilibrium in Mixtures*; Danckwerts, P. V., Ed.; International series of monographs in chemical engineering; Pergamon press: Oxford, 1969.
(24) Schwarzenbach, R. P.; Gschwend, P. M.; Imboden, D. M. *Environmental Organic Chemistry*; 2nd ed.; John Wiley & Sons, Inc.: Hoboken, 2003.
(25) Ni, N.; Yalkowsky, S. H. Prediction of Setschenow constants. *Int. J. Pharm.* **2003**, *254*, 167–172.
(26) Xie, W.-H.; Shiu, W.-Y.; Mackay, D. A review of the effect of salts on the solubility of organic compounds in seawater. *Mar. Environ. Res.* **1997**, *44*, 429–444.
(27) Weiss, R. F. Carbon dioxide in water and seawater: The solubility of a non-ideal gas. *Mar. Chem.* **1974**, *2*, 203–215.
(28) Lin, H.; Duan, Y.-Y. Empirical correction to the Peng–Robinson equation of state for the saturated region. *Fluid Phase Equilibria* **2005**, *233*, 194–203.
(29) Lohrenz, J.; Bray, B. G.; Clark, C. R. Calculating viscosities of reservoir fluids from their compositions. *J. Pet. Technol.* **1964**, 1171–1176.
(30) Privat, R.; Jaubert, J.-N. Addition of the sulfhydryl group (SH) to the PPR78 model: Estimation of missing group-interaction parameters for systems containing mercaptans and carbon dioxide or nitrogen or methane, from newly published data. *Fluid Phase Equilibria* **2012**, *334*, 197–203.
(31) Abdelrahim, M. Measurement of interfacial tension in hydrocarbon/water/dispersant systems at deepwater conditions. Master thesis, Louisiana State University, 2012.

(32) de Hemptinne, J. C.; Dhima, A.; Zhou, H. The importance of water-hydrocarbon phase equilibria during reservoir production and drilling operations. *Rev. Inst. Francais Pet.* **1998**, *53*, 283–302.
(33) Oliveira, M. B.; Coutinho, J. A. P.; Queimada, A. J. Mutual solubilities of hydrocarbons and water with the CPA EoS. *Fluid Phase Equilibria* **2007**, *258*, 58–66.
(34) Burant, A.; Lowry, G. V.; Karamalidis, A. K. Measurement of Setschenow constants for six hydrophobic compounds in simulated brines and use in predictive modeling for oil and gas systems. *Chemosphere* **2016**, *144*, 2247–2256.